EXPERIMENTAL STUDY OF GEOMETRIC VARIATIONS EFFECT ON THE FLOW PATTERNS ON A HAMMERHEAD SATELLITE LAUNCH VEHICLE

Josenei Godoi de Medeiros*, Ana Cristina Avelar, João Batista Pessoa Falcão Filho**,**
Instituto Tecnológico de Aeronáutica (ITA), Instituto de Aeronáutica e Espaço (IAE)*
São José dos Campos, SP, Brazil.

Keywords: *Launch Vehicle, Shock waves, Pressure Sensitive Paint (PSP), Schlieren.*

Abstract

The flow patterns on the frontal part of a hammerhead-type fairing launcher vehicle is experimentally analyzed for Mach number values ranging from 0.6 to 1.0, and zero angle of attack. The region of interest on the wind tunnel is characterized by three distinct sections: a rounded tip followed by a frustum cone, a constant diameter segment for the satellite compartment, a boat-tail shape sector to adjust the geometry to the following stage, and a limited length of this last propulsive stage of the vehicle. The effects of geometry modifications of the boat-tail sector on the pressure field over the model are analyzed for different values of Mach number. The experiments were conducted in the Pilot Transonic Wind Tunnel (TTP), which is located in São José dos Campos, at the Institute of Aeronautics and Space (IAE) and the techniques of Pressure Sensitive Paint (PSP) and Schlieren Flow visualization were used for obtaining pressure fields and the patterns of shock or expansion/compression waves over the model. The results obtained show that variations of the boat tail angle have a significant effect on the pressure distribution over the vehicle and on shock wave flow patterns, and consequently on drag coefficients of the vehicle.

1 Introduction

The hammerhead-type was the case of the first Brazilian Satellite Launch Vehicle (VLS-1).

Vehicles with the hammerhead-type fairing structure are a very interesting subject of studying in the transonic regime because of complex flow phenomena taking place in this speed range [2] since the geometry leads to flow separation, which can expose large areas of the vehicle to strong pressure fluctuations [3]. Accordingly, higher structural loads may take place over this region. For this reason, in the design phase, VLS-1 models have being intensively tested in wind tunnel for evaluating both the aerodynamics performance of the actual geometry as well as for validation of numerical codes.
In the present study the main purpose is to establish an experimental methodology for getting insights on complex flow phenomena in the Pilot Transonic Wind Tunnel of the *Instituto de Aeronáutica e Espaço* (IAE) making use of the techniques Pressure Sensitive Paint (PSP) and *Schlieren* flow visualization.

A 1:37 scaled model of hammerhead VLS-1 fairing, Fig. 1, was chosen in the present study. This part of the vehicle is exposed to large areas of flow separation and high-pressure gradients in flight conditions.

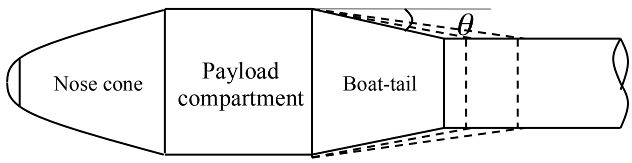

Fig. 1. Schematic representation a hammerhead shaped fairing [4].

The influence of frustum cone angle, θ, an adapting boat-tail section, Fig. 1, called here boat-tail angle is investigated in a transonic wind tunnel for Mach number values ranging from 0.6 to 1.0 and zero angles of attack.

Giving continuation to a previous work [4], which dealt with the problem using just the Pressure Sensitive Paint (PSP) technique, a more detailed analysis is presented here using in addition the *Schlieren* flow visualization, which allows more insights about the shock wave formation patterns over the model. As in the previous study, few pressure taps were used as well for validation of PSP data.

1.1 The Pressure Sensitive Paint Technique

The Pressure Sensitive Paint (PSP) is a well-established technique for measuring static pressure distribution on wind tunnel models in several important research institutions around the world. It is commonly used for steady pressure measurements and more recently applied also for non-stationary measurements, providing important insights into complex flow phenomena that cannot be resolved by the discrete pressure taps [5].

The PSP working principle is well documented in the literature [6, 7, 8] and it is based on an oxygen-quenching process in which excited molecules are deactivated by oxygen molecules. The PSP paint is composed of an oxygen-permeable polymer binder containing luminescent oxygen-sensitive molecules. When illuminated at an appropriate wavelength, the luminescent molecules become electronically excited to an elevated energy state. These molecules can return to the ground state through a radioactive process, luminescence, or non-radioactive way through release of heat. In some materials, oxygen can interact with the luminescent molecules such that the change to the ground state can be non-radioactive, and takes place by colliding with an oxygen molecule, a process known as "oxygen quenching" [7]. The more oxygen molecules available, the more quenching processes occur, which means that luminescence intensity is inversely proportional to oxygen concentration [9]. This phenomenon produces different degrees of luminosity on the model surface. The oxygen concentration, in its turn, is directly proportional to the oxygen partial pressure and, according to Henry's law [6], also to static fluid pressure. If the test surface under study is immersed in an atmosphere containing oxygen (e.g. air), the recovered luminescence intensity can be described by the Stern-Volmer equation [10].

$$\frac{I_0}{I} = 1 + K_{SV} P_{O_2} \qquad (1)$$

Where I_0 is the luminescence intensity in the absence of O_2 (i.e. vacuum), I is the luminescence intensity at some partial pressure of oxygen P_{O2}, and K_{SV} is the Stern-Volmer constant.

In wind tunnel applications, a modified form of the Stern-Volmer equation is typically used. This form replaces the vacuum calibration, I_0, with a reference standard

$$\frac{I_{REF}}{I} = A(T) + B(T)\frac{P}{P_{REF}} \qquad (2)$$

Where I_{REF} is the recovered luminescence intensity at a reference pressure, P_{REF}.

A(T) and *B(T)* are temperature dependent constants for a given PSP formulation and are usually determined previously using laboratory calibration procedures, in which the functional relationship between luminescent intensity from a paint and the pressure and temperature experienced is determined using a calibration chamber. In this procedure, a small coupon, in general in aluminum, is painted with the PSP paint and mounted onto the calibration chamber and the calibration is carried out for different values of temperature, pressure and excitation luminous intensity.

There are two approaches for acquiring PSP data. The first is the "intensity-based" technique. In this method, I_{REF} is typically acquired while the wind tunnel is turned off, and P_{REF} is the static pressure when no wind is applied. The luminescence intensity I is recovered at a determined pressure P.

The second approach, which was used in this study, is the "lifetime-based" PSP [6]. The paint is excited to fluoresce using a short illumination pulse, in general a pulsed Light Emitting Diode (LED) or Laser. Data are acquired in two different windows. The first of these windows occurs during the illumination pulse and the second is centered on the decay of the fluorescence. The signal from the first gate is sensitive to intensity of the illumination pulse and relatively insensitive to pressure. The second gate is sensitive to the intensity from the illumination pulse and very sensitive to pressure. By taking the ratio of the signal from the two gates, illumination intensity is removed and the resulting ratio signal is sensitive to pressure. The position of the gates is selected to optimize the pressure sensitivity of the system while maintaining a favorable signal-to-noise ratio. The pressure is derived from the ratio of the two images using an a priori or in situ calibration. Among the advantages of the lifetime approach is the elimination or minimization of illumination errors as described previously.

1.2 *Schlieren* Flow visualization

Flow visualization experiments using *Schlieren* is commonplace in transonic wind tunnels. The method is based on visualization of the light intensity variation as a function of the local density gradient in the flow field. A comprehensive description of this technique is given in [11]. Fig. 2 presents a schematic representation of the *Schlieren* system used in the present study.

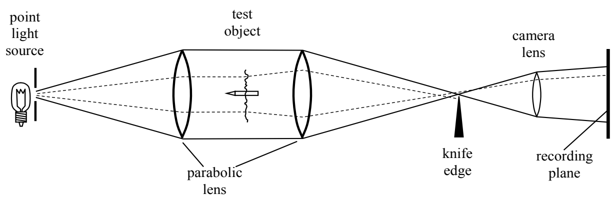

Fig. 2. Schematic representation of the Schlieren system in the TTP tunnel [12].

The point light source located precisely at the focal point of the first parabolic lens forms a parallel light beam that crosses the test object region. Different density regions refract in different ways the light beam because of the refrangibility degree variation in the local medium. Consequently, the image on the recording plane will illustrate the high density regions with shadows close to more illuminated areas. The Schlieren method uses another parabolic lens to converge light rays at the focal point where a knife edge is approximated, and as its location is altered it changes the image contrast, as it blocks some of the light rays which was diverted from the focal point. The combination of the two parabolic lenses produces an image with illumination rate as function of density gradient. Fig. 2 shows in dashed lines two light rays that experienced symmetric deflections because of density variation in the flow field. The knife selects one direction to obtain an image contrast. Both lens work together to give an image in which the luminosity is a function of the first derivative of the density in the field [12].

2 Experimental Analysis

2.1 The transonic wind tunnel

The test campaign was carried out in the Pilot Transonic Wind Tunnel (TTP) of the Institute of Aeronautics and Space (IAE), in São José dos Campos, Brazil. TTP has a test section that is 30 cm wide, 25 cm high and 80 cm length, with slotted walls to reduce shock reflection from the walls. The tunnel has a conventional closed circuit, continuously driven by a main compressor of 830kW of power, and with an intermittent injection system that operates in a combined mode, for at least 30 seconds.

A picture of TTP frontal view is shown in Fig. 3.

Fig. 3. TTP frontal view with the plenum chamber open.

TTP has automatic pressure controls from 0.5 bars to 1.2 bars, with Mach number varying between 0.2 and 1.3 as well as control of temperature and humidity in its test section, which allow stable conditions in terms of velocity, pressure and stagnation temperature.

The wind tunnel model was based on the dimensional specifications of the Brazilian Satellite Launch Vehicle VLS-1 and built on a scale 1:37 to be fitted in TTP test section with a low blockage area ratio of 1.1%. In order to allow the use of different measurement techniques and to be easy to handle during geometric configuration changes, the model was constructed with four parts, as shown in Fig 4. The boat-tail is the interchangeable part of the assembly, with five different options of angles 4^o, 8^o, 16^o, 32^o and 90^o. The connections between the parts are made through screws. In the present study the configurations with 4^o, 16^o, 32^o and 90^o were considered.

(a)

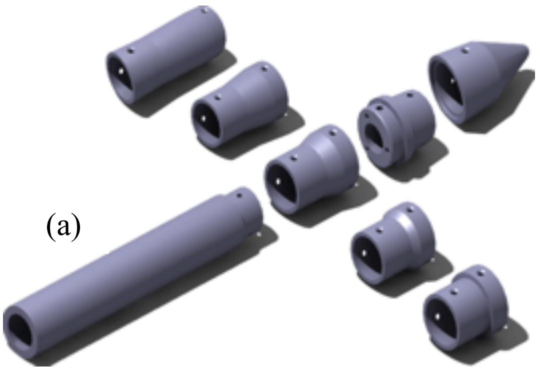

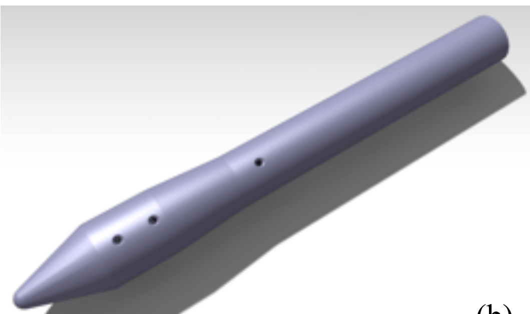

(b)

Fig. 4. a) Wind tunnel model disassembled, showing all boat-tail section configurations, b) and the model assembled for wind tunnel tests.

In spite of being a powerful facilty, TTP has some limitations for being a Pilot wind tunnel. Since the pressure range in TTP circuit is varied from 0.5 bar a 1,2 bar, the maximum Reynolds number value $5x10^5$, which is considerably lower than the Reynolds number attained by a microsatellite launch vehicle, for example, which can be higher than $2x10^7$ in an Mach number of 0.9 [13].

Due to TTP's operating Reynolds number, a rather unusual combination of laminar boundary layer at transonic flow is achieved in most conditions. As a result, aerodynamic behavior can be different from what is expected at this flow speed range for traditional aerospace applications, since most data available is based on higher Reynolds numbers, in which boundary layers are mostly turbulent already. A discussion on the effects of this laminar boundary layer on the shock wave pattern over an airfoil is presented in [9]. In the experiments reported here, a transition strip, Fig. 5, was used for inducing the boundary layer transition and this way to simulate the flow in a condition of higher Reynolds number. As suggested by [14], the transition strip, made of carborundum grains, was positioned in location correspondent to 10% of the length the nose cone of the vehicle.

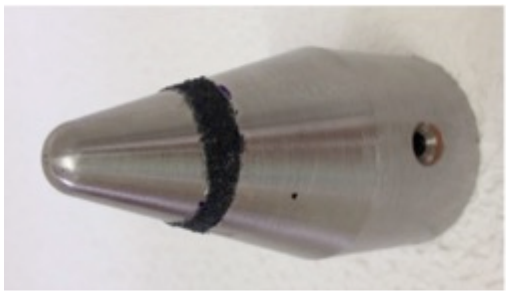

Fig. 5. Transition strip on the nose cone.

For the PSP measurements, acquisition and data processing, a commercial PSP system from Innovative Scientific Solutions, Inc. (ISSI) has been used. The UniFIB paint from Innovative Scientific Solutions, Inc. (ISSI), with has porphyrine as the oxygen-quenched material from has been used as pressure sensor. A tiny layer of FIB basecoat (ISSI FB-200) was sprayed on the model. During the painting process air was gently blew through the holes in order to avoid blockage of the pressure taps. Once painted, the model was cured in an oven at

60 ºC for 90min. A 400nm frequency LED (Light mission Diode), LM2X-DM-400 was used for exciting the luminophores. The images were acquired by using a PCO 1600 14 bit cooled CCD camera with 1600 x 1200 pixels of resolution fitted with a Nikkon lens *f#* 2.8 with focal length of 35mm. A Quantum Composer 9600+ pulsed generator was used for the synchronism between the camera, illumination system and the computer, and a commercial system from ISSI was used for data acquisition and analysis.

Image of the model painted with the PSP paint and installed in the TTP test section are shown in Fig. 6.

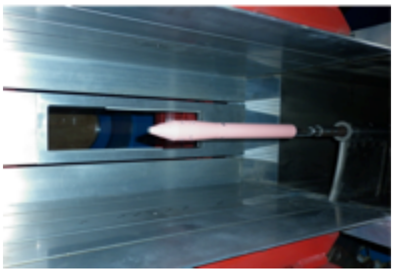

Fig. 6. Model painted with PSP and installed in the TTP test section.

Regarding the flow visualization with Schlieren, the main components of the system used are two 6” diameter parabolic mirrors, two 8” diameter flat mirrors, one knife edge, and a CCD camera PCO 1600, the same used for acquiring the PSP images. The light source was a point white light with a diverging beam and basic adjustments, which allow the center of the beam to be directed to the first of two parabolic mirrors and the source to be positioned at the focal point of the first parabolic mirror. This parabolic mirror focuses the light beam into parallel rays, which are directed toward the first flat mirror positioned at an angle of 45^o to these rays, and which directs them to the TTP test section and chamber window, this way the parallel light beam pass through these windows. The second flat mirror is positioned on the opposite side of the tunnel and directs the parallel light beam toward the second parabolic mirror, which collects and directs the light beam toward the knife-edge, where they are focused to a point, and goes on through the CCD camera [10]. The *Schlieren* system used in TTP is presented in Fig. 7.

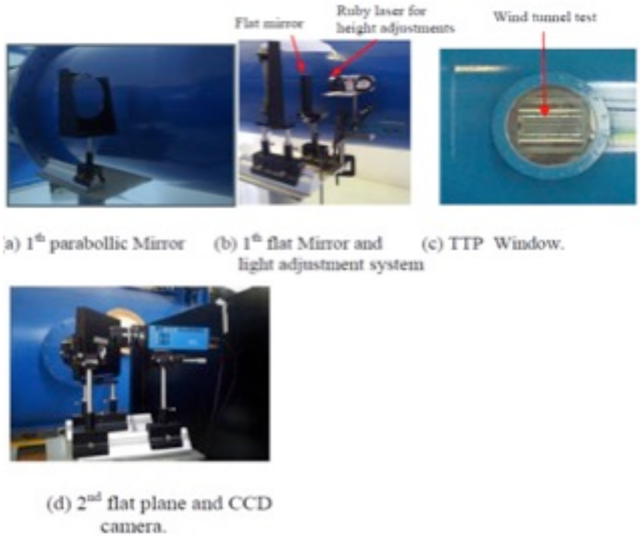

Fig. 7. Schlieren system set up in TTP.

3 Results and discussions

In this section, PSP results and *Schlieren* images for the several conditions of the boat-tail angle studied are shown. *Schlieren* images were obtained just for the boat-tail angles of 8^o, 16^o and 90^o with increments in Mach number of 0.1, starting in M=0.6 and going up to the tunnel limit of M=1.1. Some chosen *Schlieren* images and PSP flow fields are presented here to show the variations in the pressure and shock wave formation patterns in function of the geometric variations resulted from the variation of boat-tail angle.

In the previous study [4], PSP pressure field was analyzed for several values of boat-tail angle and Mach number. Here, *Schlieren* images are presented in order to get more insights in the flow patterns observed from the PSP results.

In Fig. 8, Fig. 9 and Fig. 10, PSP results and *Schlieren* images are presented for the boat-tail angle of 16 degrees and Mach numbers of 0.6, 0.8 and 1.0, respectively. In these pictures, it can be observed that the transition strip disturbs the flow and consequently the pressure variation over the model. This disturbance is well captured by the PSP and *Schileren* results as well, as can be noted from the following images.

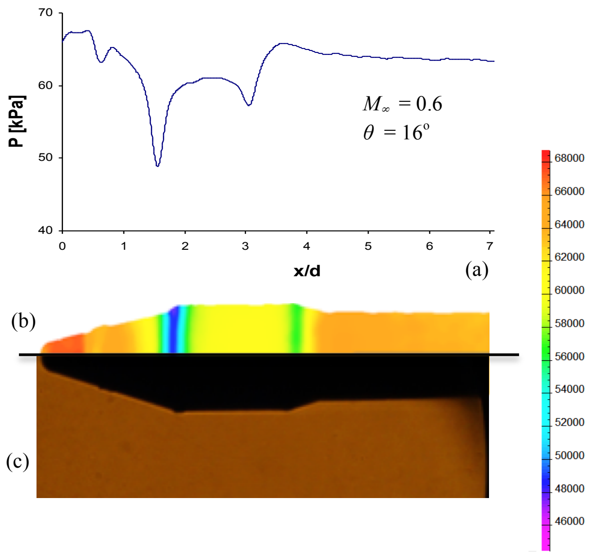

Fig. 8. PSP results and *Schlieren* Image *M*=0.6, θ=16°, (a) PSP Profile pressure in model centerline (Fig. 9b), (c) *Schlieren* Image.

From Fig. 9 and Fig. 9, at the end of the nose cone and the beginning of the payload sector a significant pressure drop is observed. The lowest pressure value in this region indicates a Mach number of about 0.87 in Fig. 8, and equal to 1.53 in Fig. 9, in this case indicating a shock wave occurrence, which can be observed in the correspondent *Schlieren* image. The pressure is recovered in the cylindrical region of the payload sector, undergoing a small decrease because of the expansion caused by the boat-tail angle. In the boat-tail sector a small pressure increase is experienced due to the diffuser effect suffered by the flow [4]. The pressure increase is more significant at the end of the boat-tail sector because of the change in the flow direction when the final cylindrical sector is reached. For the two Mach number values, *M*=0.6 and *M*=0.8, the pressure at the end of the model tends to freestream condition, reaching local Mach numbers of 0.586 and 0.803, respectively. In Fig. 10 a different flow pattern, with very strong pressure gradients is observed for Mach number 1.0, Fig. The lowest pressure value at the beginning of the payload sector indicates local Mach number of about 1.63. The flow decelerates in the payload sector up to *M*=1.21, which it is followed by a complex and long shock-wave formation. In this case, the freestream condition is not reached in the end of model. The Mach number reached in the final of the cylindrical part is 0.994. It seems that is flow is going to recover more gradually the freestream situation.

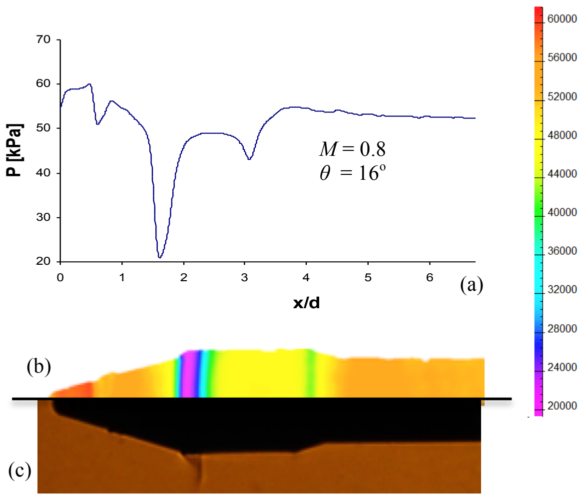

Fig. 9. PSP results and *Schlieren* Image *M*=0.8, *θ*=16°, (a) PSP Profile pressure in model centerline (Fig. 10b), (c) *Schlieren* Image.

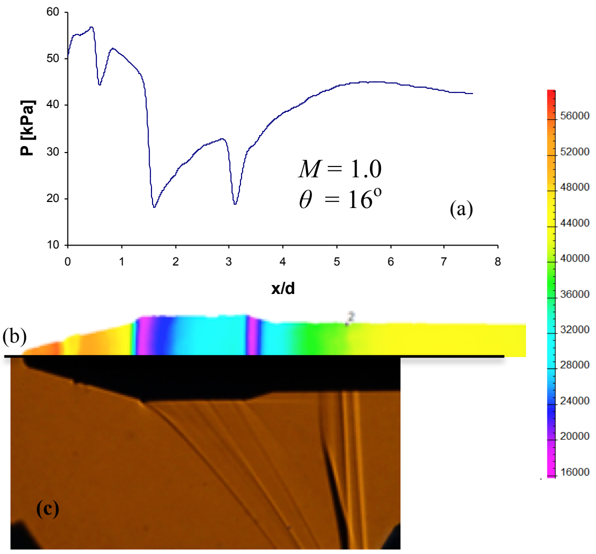

Fig. 10. PSP results and *Schlieren* Image *M*=1.0, *θ*=16°, (a) PSP Profile pressure in model centerline (Fig. 9b), (c) *Schlieren* Image.

In Fig. 11, *Schlieren* images are presented to show the shock wave development as the Mach number is increased for the boat-tail angle of 16 degrees.

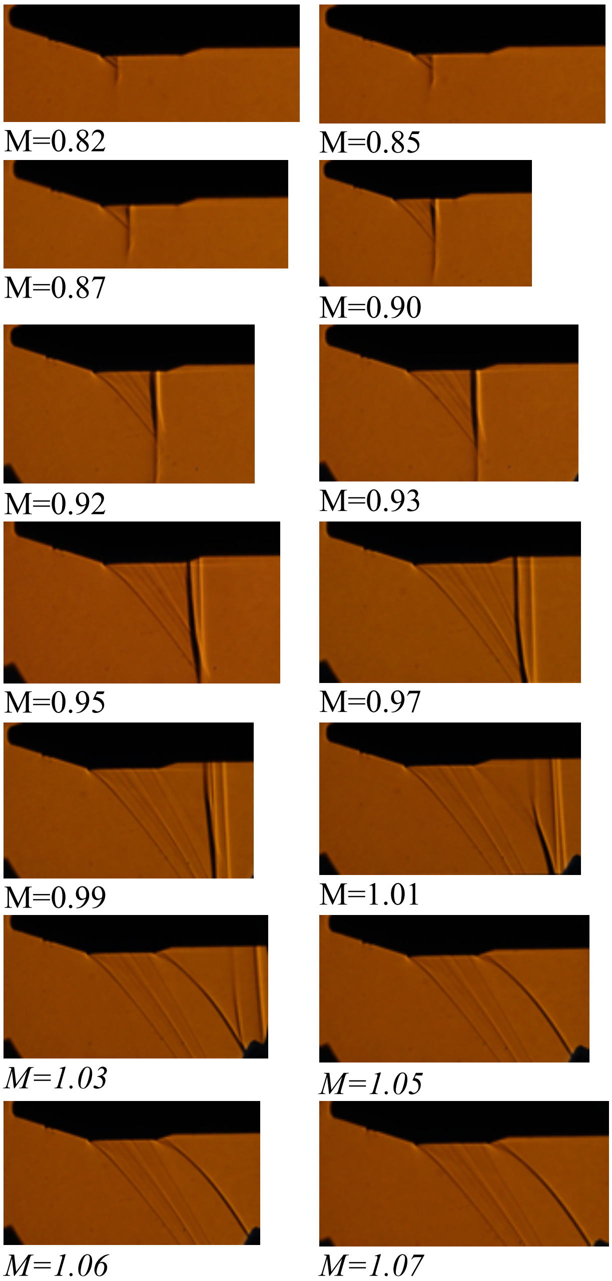

Fig. 11. *Schlieren* images showing the shock waves development as the Mach number is increased from 0.8 to 1.07 – θ =16°.

In Fig. 11, for Mach number 0.82 a normal shock wave formation in the beginning of the payload section can be clearly noted. As the Mach number increases considerable changes in the shock wave position takes place. The shock wave then propagates downstream and simultaneously and expansion waves appears upstream of the normal shock wave. At *M*=0.95 the shock wave reaches the boat-tail comportment and it seems that one more expansion wave appears. As the Mach number increases, the normal shock wave get stronger and the expansion supersonic region increases. From *M*=0.92 it seems that an oscillation of the normal shock wave position takes place.

In Fig. 12, *Schlieren* images are presented to show the flow development as the Mach number is increased for the boat-tail angle of 8 degrees.

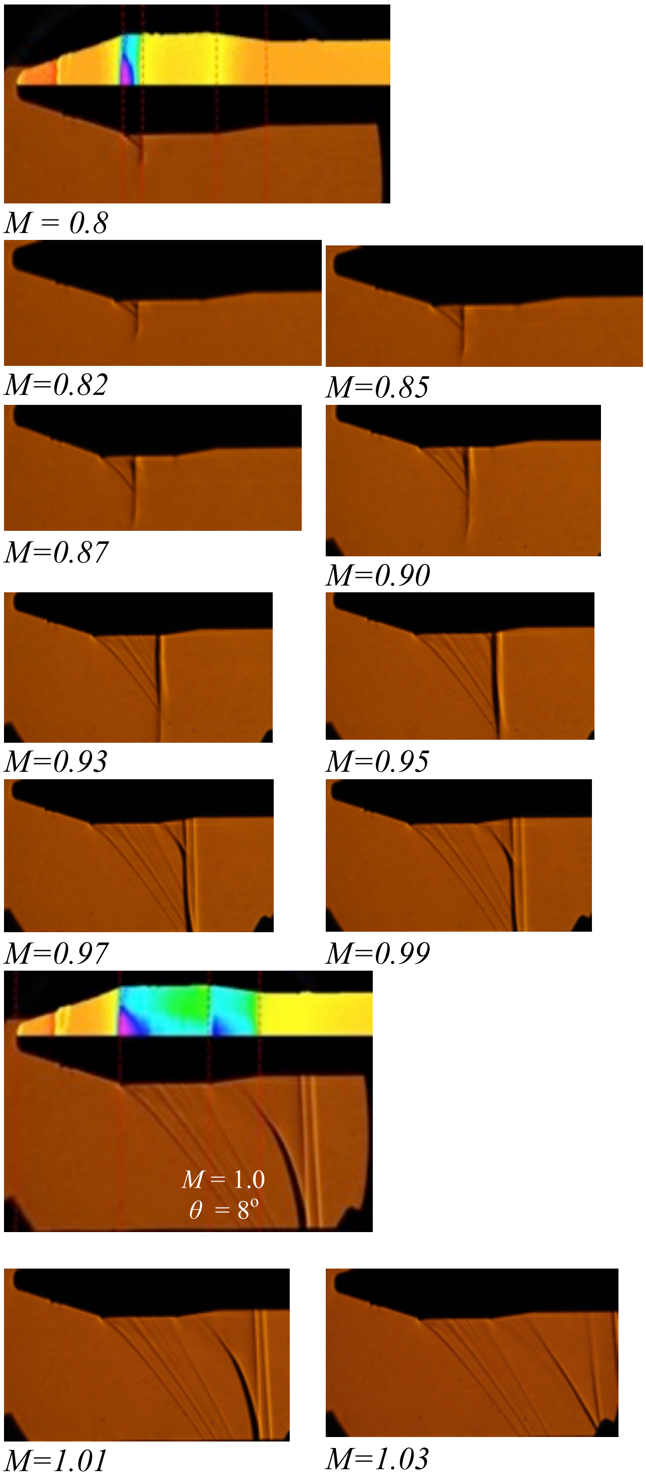

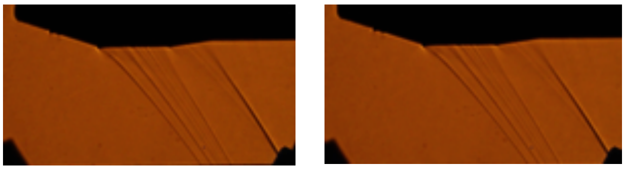

Fig. 12. *Schlieren* images showing the shock waves development as the Mach number is increased from 0.8 to 1.07 – $\theta = 8^o$.

Observing the *Schlieren* images presented in Fig.12, it can be observed that, for $\theta = 8^o$ degrees that the shock wave development patterns is very similar to what was observed for $\theta = 16^o$ up to M=0.95, which corresponds, in both cases to normal shock wave position in the beginning of the boat-tail sector. After M=0.95 the downstream shock wave propagation seems faster for $\theta = 16^o$.

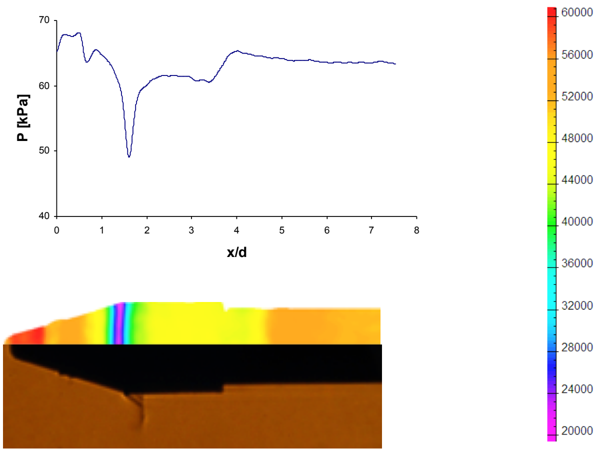

Fig. 13. PSP results and *Schlieren* Image M=0.8, θ=90°, (a) PSP Profile pressure in model centerline (Fig. 9b), (c) *Schlieren* Image.

Comparing the pressure profiles shown in Fig. 13 and in Fig. 8, it can be noted that the flow patterns in both cases are alike up to the beginning of the payload sector. Even the estimated local Mach number in this location is very similar, 0.86 (θ=16°) and 0.87 (θ=90°). In both cases the freestream conditions is reached. However, one interesting aspect is that a stronger flow deceleration is observed for θ=16°, yielding, consequently a higher-pressure gradient in this condition.

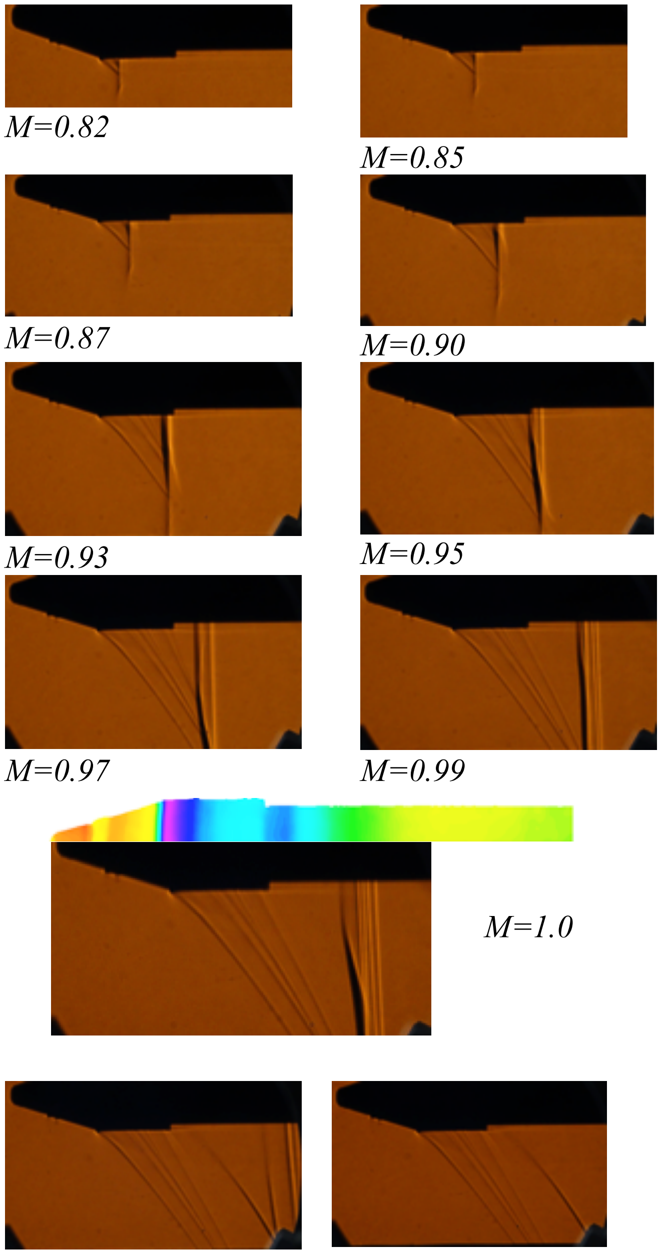

Fig. 14. Schlieren images showing the flow development as the Mach number increases from 0.8 to 1.07 – θ =16°.

Regarding θ =90°, Fig.14, it can be noted that the formation patterns of the normal shock waves and expansion waves, as well as the development of the supersonic region as the Mach number is increased, occur very similarly to the cases of boat-tail angles of 16° and 8°. Additionally, the shock wave oscillation over the model length seems to be more evident.
One interesting observation is that for θ =90°, as expected, a recirculation region, consequently

with lower pressure values is formed just after the step created by the right angle. As a result, this boat-tail angle yields higher drag coefficient, c_d, values, as can be observed in Fig. 14, but also, small pressure gradients over the model, as shown in Table 1.
In Fig. 15, drag coefficients measured with a highly precise six components internal balance are presented for several Mach number values and for the five boat-tail angles considered here, 4°, 8°, 16°, 32° and 90°. As expected, the lowest drag coefficient values are observed for the lowest Mach number values. The c_d values increases from the beginning of the transonic regime, when the influence of the wave drag is expected [15].

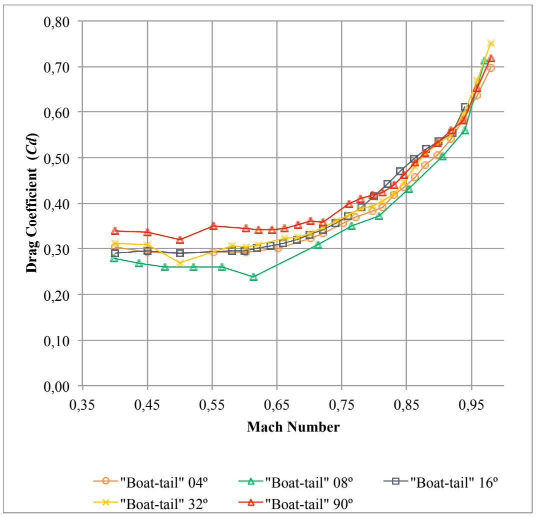

Fig. 15. Drag coefficients for the different boat-tail configurations and as the Mach number is varied.

It can be noted also from Fig. 15 that the lowest drag coefficients occur for the boat-tail angle of 8 degrees. The boat-tail of 90 degrees presented initially higher cd values, but after M=0.95, the cd values observed for this configuration were lower than the values observed for the case of 32 degrees.

Table 1 presents the main parameters observed in the pressure distribution along the model for Mach number 1.0. It is evident the highest gradients for the boat-tail angle of 16 degrees compared with the other geometries. It is also interesting observe that the boat-tail geometry that produced the lowest pressure gradients was the one with angle of 90 degrees, probably because of the low pressure region after the step created by the right angle, as mentioned before.

Tab. 1. Main parameters observed in the pressure distribution along the model for Mach number 1.0.

θ	Lowest pressure	Lowest pressure after pay-load sector	Highest pressure after pay-load sector	Highest pressure in pay-load sector	Greatest pressure ratio
4 °	19.9	30.4	48.0	34.1	2.41
16 °	18.1	18.7	47.1	32.7	2.60
32 °	18.8	27.4	44.7	31.8	2.38
90 °	21.0	29.0	46.8	34.0	2.22

These values, Tab. 1, were extracted from PSP profiles in the center line of the model. Because space limitation, not all the pressure profiles were presented here, but were shown in [4]. From Tab. 1 it can be noted that for Mach number 1.0 the pressure distribution along the model presents a meaningful difference from the subsonic cases. The lowest local pressure at the end of the boat-tail was observed for boat-tail of 16 degrees (19 kPa) and for the other geometries this value was about 28 kPa.

4 Acknowledgments

The authors thanks the Coordination for the Improvement of Higher Education Personnel (CAPES) trough the Pró-estratégia project num. 20, 2011 and the National Council for Scientific and Technological Development (CNPq) through the processes: 402233/2013-1 and 308829/2015-8 (DTI Brazil) for the financial support of the accomplishment of this research study.

References

[1] Azevedo, J L F, Moraes Jr., P, Maliska, C R, Marchi, C H, Silva, A FC (1996) Code validation for high-speed flow simulation over Satellite Launch Vehicle, *Journal of Space Craftand Rockets*, Vol. 33, No. 1, January-February.

[2] Moraes Jr., (2003) Ground and in-flight verification of the aerodynamic characteristics of the Brazilian Satellite Launch vehicle VLS.

[3] Pirk, R., Desmer, W., Pluymers, B., Sas, P.,Goes, L C S (2002) Vibro-acoustic analysis of the Vehicle Satellite Launcher (VLS) fairing, In: Proceeding ISMA 2002, Vol. 5.

[4] Avelar, A.C., Falcão Filho, J. B. P., Josenei G. Medeiros, J. G., Romero, P.G. Experimental analysis of the flow field on a hammerhead fairing satellite launch vehicle in transonic regime using Pressure Sensitive Paint (PSP), *10th Pacific Symposium on Flow Visualization and Image Processing Naples, Italy, 15-18 June, 2015.*

[5] Gregory, J. W., Sakaue, H., Liu, T., Sullivan, J. P., "Fast Pressure-Sensitive Paint for Flow and Acoustic Diagnostics," *Annu.Rev.Fluid Mech.* Vol. 46, pp. 303–30, 2014.

[6] Liu, T, Sullivan, J P (2005) Pressure And Temperature Sensitive Paints", Springer-Verlag, New York.

[7] Engler, R H, Klein, C, Trinks, O (2000) Pressure sensitive paint systems for pressure distribution measurements in wind tunnels and turbomachines, *Meas. Sci. Technol*., Vol. 11, 1077, doi:10.1088/0957-233/11/7/320.

[8] Gregory, J W., Asai, K, Kameda, M, Liu, T, Sullivan, J P (2008) A Review of Pressure Sensitive Paint for High Speed and Unsteady Aerodynamics", In: Proceedings of the Institution of Mechanical Engineers, Part G, Journal of Aerospace Engineering, Vol. 222, No. 2, pp. 249-980.

[9] Fanini, H. L., Avelar, A. C., Falcão Filho, J. B. P., Silva, R. G. A., Experimental Study of Shock Wave Patterns Over an Airfoil, AIAA Aviation, 46th AIAA Fluid Dynamics Conference, 13-17 June 2016, Washington, D.C., DOI: 10.2514/6.2016-3935.

[10]Watkins, A. N., Bradley, D. L., Lipford, W. E., Wong, O. D., Oglesby, D. M., Ingram, J. Development of a Pressure Sensitive Paint System for Measuring Global Surface Pressures on Rotorcraft Blades, 22nd International Congress on Instrumentation in Aerospace Simulation Facilities, 10-14 June 2007, Pacific Grove, CA.

[11] Tropea, C., Yarin, A. L., Foss, J. F., 2007, *Springer Handbook of Experimental Fluid Mechanics*, Springer.

[12] Da Mata, H. O., Falcão Filho, J. B. P., Avelar, A. C., Carvalho, L. M. M. O., Azevedo, J. L. F., *accept for publication at Journal of Aerospace Technology and Management – JATM* (to be published in 2016).

[13] Falcão Filho, J. B. P., Avelar, A. C., Reis, M. L. C. Historical review and future. Journal of Aerospace Technology and Management, São José dos Campos, v. 1, n. 1, jun. 2009.

[14] Pope, A., Goin, K. L. High-Speed wind tunnel testing. New York: Robert E. Krieger Publ., 1978. 322 p.

[15] Cohen, I. M., Kundu, P. K. Fluid mechanics. 4a. ed. [S.l.]: Academic Press, 2008.

5 Contact Author Email Address

anacristina.avelar@gmail.com

Copyright Statement